Low- and high-field transport properties of modulation-doped Si/SiGe and Ge/SiGe heterostructures: Effect of phonon confinement in germanium quantum wells

S. Madhavi* and V. Venkataraman
Department of Physics, Indian Institute of Science, Bangalore 560 012, India

J. C. Sturm
Department of Electrical Engineering, Princeton University, Princeton, New Jersey 08544

Y. H. Xie
Department of Materials and Applied Science Engineering, School of Engineering and Applied Science, University of California, Los Angeles, California 90024

(Received 29 December 1999)

In this paper we report experimental studies carried out on two-dimensional electrons in strained silicon and two-dimensional holes in strained germanium channel modulation doped heterostructures, to understand their low- and high-field transport properties. Hall measurements were done to determine the low-field Ohmic mobility as a function of temperature (13–300 K). Geometric magnetoresistance technique was used to measure the mobility as a function of the applied field up to 300 V/cm for lattice temperatures from 13 to 200 K. We observe that at high fields the mobility decreases at a faster rate in the germanium channels compared to silicon channels. Numerical calculations based on standard transport theories for low-field transport and nonlinear transport at high fields are also presented. We propose that the faster mobility decrease in germanium is due to local heating of confined phonons owing to acoustic mismatch with the cladding layers. We also present results based on the transient response of the lattice heating effects in both silicon and germanium systems as a function of the duty cycle of the applied electric field, which confirms the role of the local phonon temperature in the germanium quantum well.

I. INTRODUCTION

Over the years, advancement in growth techniques have led to an improvement in the low-temperature Ohmic mobilities of two-dimensional electron gas (2DEG) in strained silicon channels to nearly 5×10^5 $cm^2/V\,s$ and in two-dimensional hole gas (2DHG) in strained SiGe channels to nearly 1×10^4 $cm^2/V\,s$.[1–3] Recently there have been a few reports on high mobility 2DHG in strained pure germanium channels[4–6] with peak mobilities reaching $6\times10^4 cm^2/V\,s$. Such high hole mobilities in pure germanium channels are of considerable interest for *p*-modulation-doped field-effect transister (MODFET) devices. However, at high operating electric fields, the mobility of these systems decreases from its Ohmic value owing to energy dependent scattering between the 2D carriers and the phonons. The carriers initially gain energy from the field at a higher rate, until balanced by the rate of loss of energy to the lattice by collisions, so that in steady state the mean energy of the carrier gas is increased. This causes an increase in the carrier temperature and a reduction in the 2D carrier mobility. Such ''hot carrier'' transport in high-electric fields has been studied extensively in GaAs-AlGaAs heterostructures, but few reports exist so far in Si-Ge heterostructures.[7–10] It is important to study the hot-carrier behavior in these systems not only to determine the device properties but more importantly to understand the mechanism of energy relaxation due to carrier-phonon interactions at high fields and also the energy-transfer characteristics between the source-carrier-phonon systems. This study brings out a clear picture of the contribution of different scattering mechanisms involved in both momentum and energy relaxation in these systems.

High-field behavior in GaAs-based systems was earlier studied using either Shubnikov de Haas effect or by measuring the drain current in FET geometry. The first measurement on high-field saturation drift velocity in two-dimensional carrier gases in silicon systems was reported by Cooper and Nelson[11] in 1981 using the time-of-flight method in Si inversion layers. Ismail *et al.*[12] have reported saturation drift velocities at high fields in modulation doped Si heterostructures from FET characteristics. Song *et al.*[8] and Xie *et al.*[5] have earlier reported experimental data on hot carrier effects in 2D Si, Ge, and SiGe systems at low temperatures ($\sim$4.2 K) by Shubnikov de Haas measurements. Most of these experiments were limited to very low temperatures or involved an indirect measurement of the mobility by assuming the carrier concentration in the quantum well. In this paper we determine the high-field characteristics in Si and Ge 2D systems by directly measuring their mobility using geometric magnetoresistance technique (GMR), which was earlier used by Masselink *et al.*[10] in 1985 to study the high-field transport in GaAs-AlGaAs systems. This technique is suitable to measure the mobility even close to room temperature and does not require very high magnetic fields or any assumption of the carrier density in the quantum well. The magnetoresistance is proportional to the square of the mobility[10] and hence, the signal weighs the high-mobility 2D carrier system more than the rest of the bulk substrate.

Most of the earlier theories on hot carrier transport were based on the semiclassical Boltzmann transport equation. When the system goes beyond the linear regime, solution of the Boltzmann equation becomes a laborious task and one

TABLE I. Details of the structures of the samples reported. In the case of sample #B and #C the delta doping density (cm^{-2}) is mentioned.

Sample	Channel	Buffer	Spacer (Å)	Doping density	Well width (Å)
A(#922)	Si	$Si_{0.62}Ge_{0.38}$	80	2×10^{19} cm^{-3}	75
B(#348)	Ge	$Si_{0.2}Ge_{0.8}$	200	1×10^{12} cm^{-2}	250
C(#324)	Ge	$Si_{0.4}Ge_{0.6}$	200	1.1×10^{12} cm^{-2}	70

has to resort to approximate methods like the electron temperature model (ETM) which uses a Maxwellian distribution function to describe the nonequilibrium carrier system characterized by the carrier temperature. Strictly speaking, one cannot define a temperature for transport electrons that are not in the equilibrium state. It is therefore necessary to distinguish mean energy of the relative carrier system characterized by its temperature and the energy associated with the drift motion of the entire carrier system. An accurate method to describe the steady-state transport in high fields based on the Green-function approach was given by Lei and Ting[13,14] in 1985, which is more suitable to study high mobility systems where the drift velocity is sufficiently large that it cannot be neglected in comparison to the mean energy of the carrier system. In this paper we studied the high-field behavior of our Si–Ge systems based on both these approaches and find that the model by Lei and Ting is more suitable to explain high-field transport in these systems.

High-electric fields in devices are known to cause degradation of mobility due to a combination of high-carrier temperature (''hot'' carrier effect)[7] and increased lattice temperature. Pulsed electric fields with very small duty cycle (ratio of pulse width to period) have been used so far to eliminate these lattice heating effects and isolate the mobility dependence on carrier temperature. Such a procedure is well justified for bulk semiconductors and lattice matched heterostructures like AlGaAs/GaAs[15] where good thermal coupling between the carrier system and the large heat capacity substrate gives rise to slow thermal time constants ($\sim$ milliseconds). Hence a reduction of the duty cycle to 1%–2% lowers the average power dissipation and lattice heating. However, in the case of Si/Ge quantum well heterostructures, we find from our experimental investigation that significant acoustic mismatches across interfaces can give rise to local heating effects inside the quantum well that are significant even with small duty cycle pulses ($\sim$2%). In this paper, we also present systematic experimental data of the dependence of hot carrier mobility on pulse width and frequency to study the transient heating response in these systems and explain their characteristic small response times to be the effect of confined phonons.

This paper is divided into five sections. In Sec. II we discuss the experimental procedure including details of sample structure, measurement techniques, and experimental conditions. In Sec. III, we outline the results obtained from the low- and high-field studies and also discuss the results giving details of the calculations involved. In Sec. IV, we present details of the experimental procedure and also the results obtained from the transient lattice heating measurements. Finally, in Sec. V we summarize the main points of our results.

II. EXPERIMENT

The silicon quantum well samples were grown by rapid thermal chemical vapor deposition.[16] The samples (#A) were grown on *p*-type wafers ($\sim$10 Ωcm). The relaxed graded buffer layer was grown at 625 °C consisting of 0%–38% increase by composition of Ge up to 2600 Å. A 6000 Å uniform $Si_{0.62}Ge_{0.38}$ layer annealed relaxed buffer was then grown. A 75 Å silicon channel was grown at 700 °C over the relaxed buffer followed by 80 Å of *i*-layer spacer capped with 300 Å of 2×10^{19} cm^{-3} phosphorous doped layer.

The Germanium samples (#B and #C) were grown on a relaxed buffer by molecular beam epitaxy.[17] The substrate was *p*-type Si (100) with resistivity $>$50 ohm cm. In the case of sample #B, the relaxed buffer consists of 10% Ge increase per micron of *i* layer and a 1.5 μm uniform 80% Ge undoped cap. The active region consists of a boron delta doped layer of $\sim1\times10^{12}$ cm^{-2}, a 200 Å spacer layer, a 250 Å Ge channel, a 530 Å upper spacer *i* layer, a boron delta doping of $\sim9\times10^{11}$ cm^{-2} for compensating the band bending at the surface and finally a 200 Å *i* layer as the cap. All the layers except the channel have the composition of 80% Ge. Sample (#C) is grown on a similar substrate as #B. The relaxed buffer consists of 10% Ge increase per μm to 60% Ge and a 1.5 μm of undoped 60% Ge cap. All layers except the channel have 60% Ge. The active region is similar to sample #B, except that the bottom delta doping is 1.1×10^{12} cm^{-2}, the Ge channel width is 70 Å, and the upper delta doping density is 1.6×10^{12} cm^{-2} of boron. In both the samples between the relaxed buffer and the active region there is a chemical mechanical polishing step to remove the cross-hatched pattern from the surface. Table I gives the relevant details of the sample structures reported in this paper.

For the low-field measurements, the samples were patterned into 3 mm$\times$3 mm squares. In the case of the *n*-type electron gas samples, the Ohmic contacts were made by depositing AuSb at the corners in Van der Pauw geometry and annealing the contacts at 250 °C . For the *p*-type hole gas samples, Ohmic contacts were made by depositing AuGa and annealing at 300 °C. The contacts were annealed such that they remained Ohmic for temperatures ranging from 13 up to 300 K. Hall measurements were carried out to measure the carrier concentration and mobility as a function of temperature.

In order to study the high-field transport properties, the samples were processed into ungated FET geometry with the channel length (25 μm) to width (500 μm) ratio very small ($<$0.05), which is a very good approximation to the Corbino disk geometry. Ohmic contacts were made by depositing AuSb on Si samples and AuGa on Ge samples. The

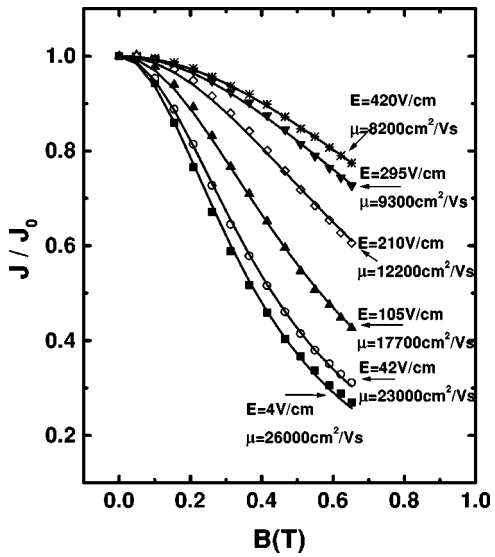

FIG. 1. The magnetic-field dependence of the normalized current density through the Ge channel (#B) for different values of the applied electric field at 13 K. The lines show the GMR fits with the mobility as the fitting parameter.

metallization and annealing were carried out as mentioned before so as to obtain low-resistance Ohmic contacts. The low-contact resistance is very essential for these two terminal magnetoresistance measurements as the narrow channels themselves have very low resistance ($\sim 5\ \Omega$) at low temperatures (~ 13 K). The resistance of the channel for all samples decreased with a decrease in temperature, which is characteristic of modulation doped heterostructures.

Voltage pulses of 2% duty cycle (width 200 μs and period 10 ms) were applied to avoid lattice heating. Experimental results to study lattice heating by varying the duty cycle are described in Sec. IV. The applied electric field ($\mathbf{E}_{app}$) was determined from the voltage after correcting for contact resistance effects. This involved measuring the total resistance of the channel and the contacts (R_T) by I-V measurements and obtaining the channel resistance (R_c) from Hall determined resistivity and channel dimensions. The electric field across the 2D carrier gas is given by $\mathbf{E} = \mathbf{E}_{app}\ (R_c/R_T)$. The samples were subjected to a normal magnetic field scanned from 0–0.7 T and the change in the current through the channel with magnetic field (B) was measured. From this the GMR mobility (μ) is determined directly by fitting the expression

$$\frac{j}{j_0} = (1+\mu^2 B^2)^{-1} \tag{1}$$

to the data. In the above expression, j_0 and j are the currents through the channel in the absence and in the presence of the magnetic field B. The experimental data for sample #B along with the fit is shown in Fig. 1 for selected electric fields at 13 K. This relation holds even for nonlinear transport at high-electric fields where the mobility is defined as $e<\tau(\mathbf{E})>/m^*$ where e is the electronic charge and m^* is the effective mass. $\tau(\mathbf{E})$ is the statistical average of the relaxation time, which is a function of the electric field.

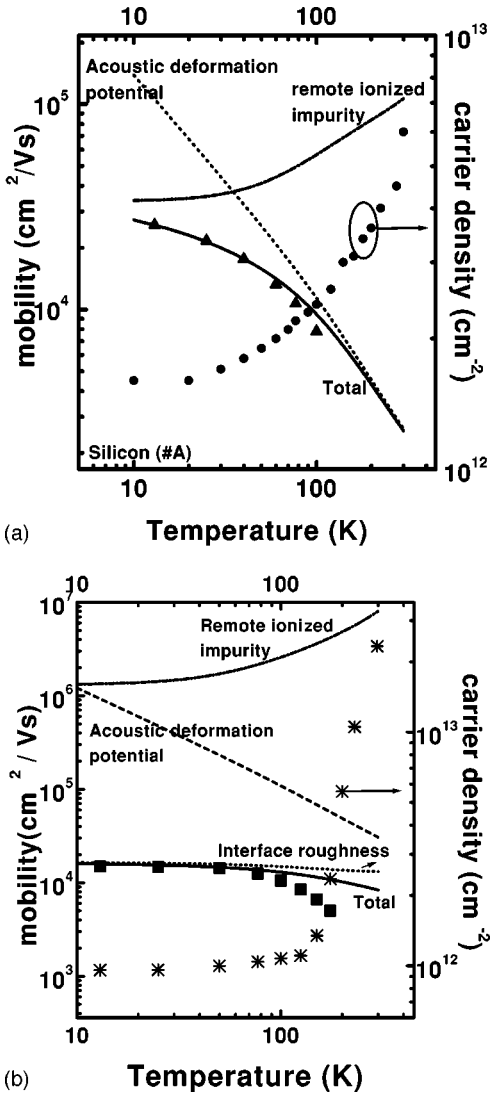

FIG. 2. The experimental mobility data (solid symbols) as a function of the temperature for (a) Si (#A) and (b) Ge (#C) samples. The dotted and dashed lines are the calculated mobilities due to the individual scattering mechanisms indicated and the solid line corresponds to the calculated total mobility. The open symbols are the experimental carrier concentration as a function of temperature.

The mobility was determined as a function of the applied electric field for different temperatures ranging from 13 up to 200 K for both the two-dimensional electron and hole gas systems.

To study the steady-state and transient thermal response, we measure the GMR mobility as a function of the duty cycle by varying both the width and the frequency of the applied electric field pulse. These experiments are discussed in Sec. IV.

III. RESULTS

A. Low-field transport

The carrier concentration and mobility of the two systems were measured by Hall as a function of temperature from 13 up to 300 K. The results are shown in Figs. 2(a) and 2(b). Table II lists the mobility and carrier concentration in the systems studied at 13 and 77 K.

TABLE II. Mobility and the carrier concentration of the 2DEG and 2DHG samples as measured by Hall. The values of the effective mass (m_t^*, m_l^*) and deformation potential constant (D) are taken from Refs. 8 and 28.

Sample	Mobility ($cm^2/V\,s$)	Carrier conc. (cm^{-2})	Effective mass (m_e)	D (eV)	u_L (m/s)
A (Si)	26000 (13 K)	1.7×10^{12} (13 K)	0.98 (m_l^*)	10	9×10^3
	10600 (77 K)	2×10^{12} (77 K)	0.2 (m_t^*)		
B (Ge)	26000 (13 K)	8.6×10^{11} (13 K)	0.2 (m_l^*)	14	5×10^3
	14000 (77K)	1×10^{12} (77 K)	0.1 (m_t^*)		
C (Ge)	15000 (13 K)	9.6×10^{11} (13 K)	0.2 (m_l^*)	14	5×10^3
	12500 (77 K)	1×10^{12} (77 K)	0.1 (m_t^*)		

The mobility remains close to its 13 K value up to 30 K for 2DEG and 70 K for the 2DHG after which it decreases with temperature. At room temperature the 2DEG sample has a mobility of 1050 $cm^2/V\,s$ and carrier density of 6×10^{12} cm^{-2} while the mobility of the 2DHG sample comes down to 500 $cm^2/V\,s$ with a carrier density of 2.3×10^{13} cm^{-2}. Beyond temperatures of approximately 77 K, parallel conduction plays a very significant role as seen from the increase in carrier concentration.

Using the procedure given by Price[18] and Hirakawa and Sakaki,[15] we calculate the Ohmic mobility as a function of temperature in these two systems, by taking into account scattering mechanisms due to acoustic phonons, remote ionized impurity, interface roughness, and optical phonons. Apart from explaining our experimental results, we also report theoretical calculations to explain the mobility curves for those data reported in literature (henceforth referred to as ''literature data''), which were taken from Refs. 19 and 5 and reproduced in Figs. 3(a) and 3(b). The procedure used in the calculation is given in Appendix A, Sec. I.

In the case of the 2DEG samples, the strain in the Si channel lifts the sixfold degeneracy of the conduction band into twofold degenerate lower valleys and fourfold degenerate upper valleys.[20] This reduces the intervalley phonon scattering in these strained layers considerably. In the case of the literature data,[19] the low-temperature mobility is limited by remote ionized impurity scattering. In our samples also the low-temperature mobility is mostly limited by remote ionized impurity scattering. Due to the very large doping density ($\sim2\times10^{19}$ cm^{-3}) and smaller spacer thicknesses (~70 Å) these samples show lower mobilities when compared to the literature data. In both cases there is lesser interface roughness compared to the Si/SiO_2 systems, and the interface roughness scattering does not play a significant role in limiting the low-temperature mobilities. The theoretical plot for interface roughness scattering is plotted for the typical roughness values in Si/SiO_2 systems ($\Delta=5$ Å and $\Lambda=10$ Å) in Fig. 3(a). Intravalley optical phonon scattering in Si is very weak and hence, does not contribute to mobility limitation even at room temperature.[21] Numerical calculations based on the aforementioned analysis was carried out to determine the mobility due to the individual scattering mechanisms and also the total mobility due to all of them as a function of temperature. The theoretical fits are shown in Figs. 2(a) and 3(a) as solid and dotted lines for total mobility and individual contributions, respectively.

In the case of the 2DHG, the strain in the Ge channel lifts the Γ point degeneracy between the heavy-hole and the light-hole bands. The two-dimensional confinement further increases the spacing between the bands.[5] Due to the balance

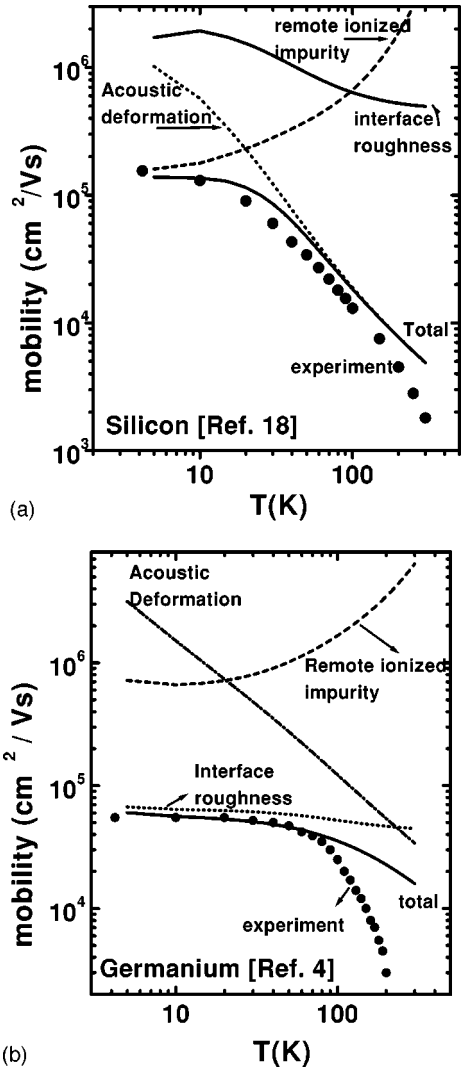

FIG. 3. The temperature dependence of mobility taken from literature for (a) SiGe/Si/SiGe (Ref. 19) and (b) SiGe/Ge/SiGe (Ref. 5) modulation doped heterostructures. The dotted and the dashed lines show the individual contributions of the different scattering mechanisms mentioned and the solid line gives the total calculated mobility.

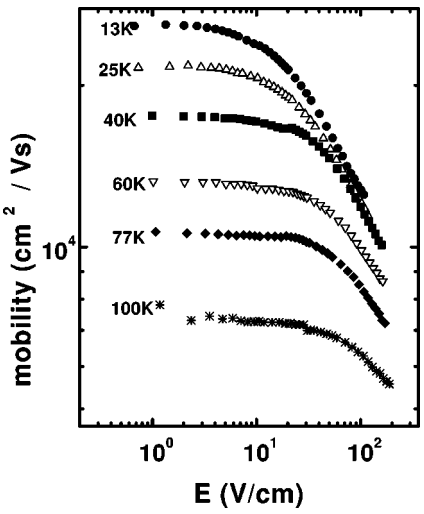

FIG. 4. Mobility of the 2DEG in strained silicon channel (#A) as a function of the applied electric field for different bath temperatures.

between the strain energy and the surface step energy of the growing Ge surface over the $Ge_{0.6}Si_{0.4}$ graded layer, the interface shows considerable roughness in these completely coherently strained structures. This was clearly visible in the cross-sectional TEM images of these structures.[5] At low temperatures the mobility is limited by scattering due to these rough interfaces. The remote ionized impurity scattering does not play a role due to large spacer thicknesses and delta doping. In the case of a large splitting between light and heavy holes, the deformation potential coupling between holes and optical phonons as well as scattering between light hole and heavy hole can also be neglected.[22] Consequently, there is an enhancement in the 300 K mobilities in these structures to above 8000 $cm^2/V\,s$. This is much larger than the 300 K bulk mobilities in Ge ($\sim$1500 $cm^2/V\,s$) which is limited by strong optical-phonon scattering. In the experimental data, above 70 K, parallel conduction through the doping layer and the *p*-type substrate effectively shunts the modulation doped channel and precludes comparison with theory. Numerical calculations based on Boltzmann theory were carried out to determine the mobility due to the individual scattering mechanisms and the total mobility as a function of temperature. The theoretical fits are shown in Figs. 2(b) and 3(b) as solid and dotted lines for total mobility and individual contributions, respectively.

B. High-field transport

The dependence of mobility on electric field for temperatures ranging from 13–200 K for the 2DEG (#A) and 2DHG (#B, #C) samples are shown in Figs. 4 and 5, respectively. It is seen that the mobility remains constant at its low-field value (μ_0) untill it reaches a critical field ($\mathbf{E}_C$) beyond which it decreases with electric field. Beyond $\mathbf{E}_C$ it is seen that the rate at which the mobility decreases with the field is different for silicon and germanium 2D systems. The high-field data for various temperatures collapse on to a single curve when the electric field is scaled with the low-field mobility (μ_0) and the high-field mobility is normalized with μ_0. The entire family of curves for different temperatures are shown in Fig. 6. The spread in the μ/μ_0 vs $\mu_0\mathbf{E}$ plots in Fig. 6 lie within the experimental error in determining the electric field after eliminating the contact resistance effects. The difference in the high-field slopes in the two systems suggests that the microscopic physics governing the energy relaxation of hot carriers is different in the two systems.

To further examine the energy relaxation mechanism we study the average energy loss rate as a function of the carrier temperature in both the systems. Numerical calculations based on energy balance equations and Boltzmann transport theory[18,23–25,27] (electron temperature model) were carried out to determine the dependence of mobility on the electric field. The calculation procedure is summarized in Appendix A, Sec. 2. The values for the acoustic deformation potential constant (D), the longitudinal (m_l^*) and transverse (m_t^*) effective masses, and longitudinal sound velocity (u_L) that were used in the calculations were taken from previously published reports[8,28] and are listed in Table II.

In the case of silicon we showed in the previous section that the mobility at low-electric fields is limited by remote ionized impurity scattering and at higher electric fields cor-

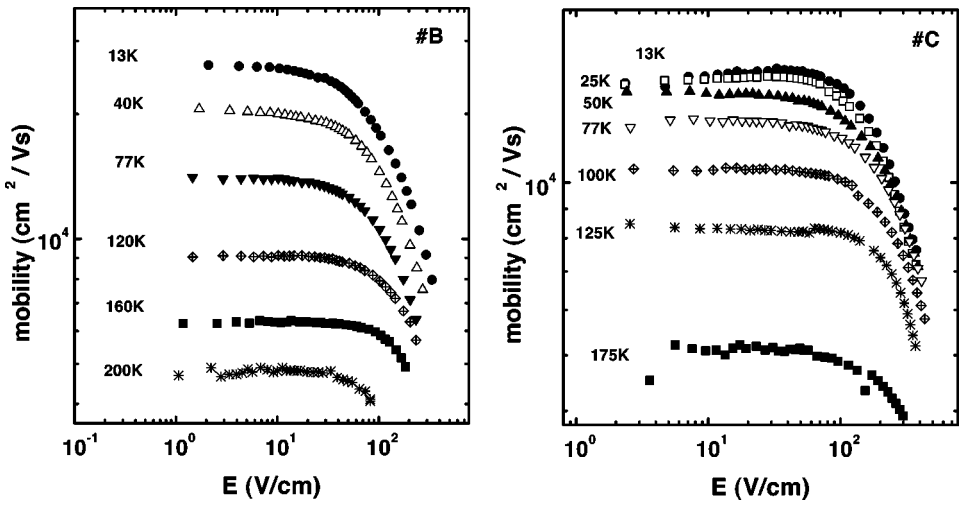

FIG. 5. Mobility of the 2DHG as a function of the applied electric field for different bath temperatures in strained germanium channel (a) sample #B and (b) sample #C.

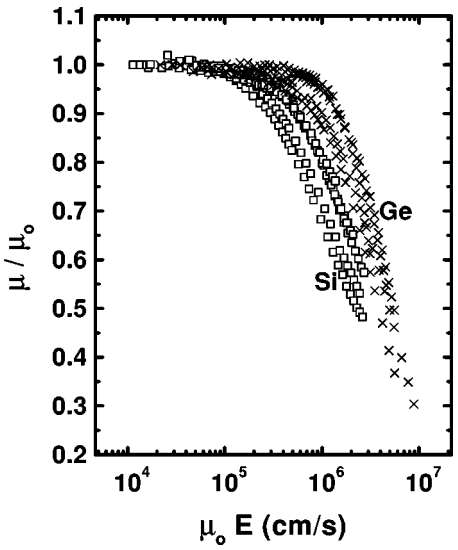

FIG. 6. Mobility normalized with respect to the low-field value (μ_0) plotted as a function of the electric field scaled with μ_0 for all temperatures measured. The square symbols are for the 2DEG in #A and the crosses are for the 2DHG in #B and #C.

responding to higher carrier temperatures the phonon scattering plays the dominant role. We calculated numerically $-\langle dE/dt\rangle$ $(=\mu e\mathbf{E}^2)$ as a function of **E** using the above procedure. μ is determined as a function of the electron temperature (T_e) using the formalism given in Appendix A, Sec. 2, where T_e is used to define the carrier distribution function instead of the lattice temperature. From these calculations we can also determine T_e as a function of **E**. This analysis, however, showed no degradation of mobility as the electric field was increased [Fig. 7—dotted line]. The failure of the ETM model to explain the experimental results can be attributed to the high mobility in our samples.

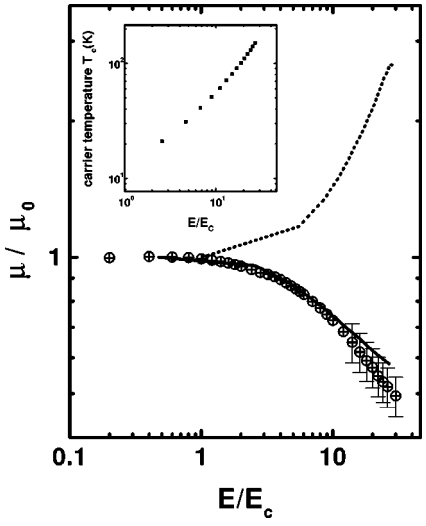

FIG. 7. The normalized mobility as a function of the applied electric field normalized with respect to E_C (4.5 V/cm) for the strained silicon channel (#A) at bath temperature of 13 K. The dotted line shows the calculated high-field behavior using ETM and the solid line corresponds to the calculation based on Lei and Ting's approach. The inset shows the calculated carrier temperature as a function of E/E_C.

This model was successful in describing the high-field behavior of low-mobility systems such as Si/SiO_2 inversion layers,[29–32] due to the fact that the drift velocity is much smaller than the spread in the velocity distribution that is determined by the temperature of the carriers. Hence, the drift velocity does not contribute much to the nonlinearity and can be neglected in the analysis. However, if the mobility of the system is large, as is the case in Si–Ge or GaAs heterostructures, the drift velocity cannot be neglected in the formulation, and should be included in describing the distribution function and in the carrier-carrier interaction. A similar conclusion was reached by Sakaki *et al.*[25] in their analysis of hot carrier mobility degradation in AlGaAs–GaAs 2DEG systems. To take into account the high-drift velocity a two parameter ''displaced'' Maxwellian distribution function incorporating both the drift velocity and the carrier temperature is used to solve the coupled momentum and energy balance equations.[26] However the assumption of a symmetric distribution function with a well-defined carrier temperature in a highly nonequilibrium situation cannot be justified rigorously.

A new method to solve the coupled momentum and energy balance equations without reference to any carrier distribution function was described by Lei and Ting[13,14] in 1985. This method is equivalent to the Boltzmann transport theory at low fields but deviates from it in the hot carrier regime. The method lies in the separation of the center-of-mass motion from the relative motion of the carriers in drift, so that the electric field acts on the center-of-mass motion only. The motion of the relative carrier system, which consists of a large number of interacting particles, is essentially a statistical movement and, together with the phonon system, is described by a statistical density matrix (ρ). An electron temperature is introduced as a measure of the internal energy of the relative carriers without reference to any distribution function. It should be noted that the electron temperature is not the only source of the nonlinearity of the mobility with electric fields; the drift velocity **v** enters the force and energy transfer expressions via the Bose factors and the electron density-density correlation function. This method was used successfully to describe the high-field transport in GaAs/AlGaAs heterostructures by Sakaki *et al.*[25] earlier. The details of the procedure are given in Appendix B.

In the weak current limit($v\rightarrow 0$) the solution of the energy balance equation is $T_e = T_L$ and Ohmic resistivities can be obtained directly. We obtain the same results numerically as we obtain using the Boltzmann transport theory in the low-field case.

Using the above-mentioned formalism we can calculate numerically μ and T_e as a function of **E**. In the case of Si, we have performed calculations based on this approach, using similar parameters as used in the Boltzmann analysis, and have obtained the solid curve in Fig. 7. The inset shows the calculated values of T_e as a function of the electric field. We obtain a carrier temperature of approximately 100 K at an electric field of approximately 100 V/cm, which is of the same order as that obtained for AlGaAs-GaAs heterostructures.[33,34] The slope of the experimentally measured high-field mobility versus electric-field curves are very similar to the theoretically calculated curves, suggesting that at high fields the energy relaxation is dominated by acoustic

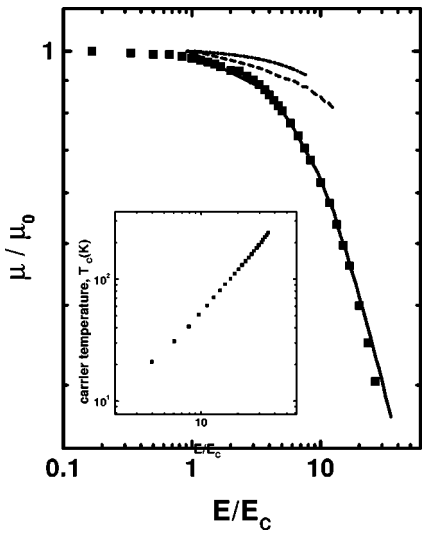

FIG. 8. The normalized mobility as a function of the applied electric field normalized with respect to E_C (5V/cm) for the strained germanium channel (#B) at bath temperature of 13 K. Also shown are calculated high-field behavior using ETM (dot-dash line), Lei and Ting's approach using $T_{ph}=T_{bath}$ (dotted line), and using $T_{ph}>T_{bath}$ (solid line). The inset shows the calculated carrier temperature as a function of E/E_C.

phonons through deformation potential scattering. The calculated critical electric field ($\mathbf{E}_C$) at which the mobility starts decreasing, agrees within a factor of 2 with the experimental data. This discrepancy lies within the experimental error involved in the estimation of the electric field in the channel.

In the case of germanium (#B), a similar analysis as performed in the case of silicon did not show a qualitative difference in the high-field behavior [Fig. 8—dotted line]. We find that the calculated rate of decrease of mobility is the same as in the silicon case, but not faster as seen from experiment. This discrepancy between theoretical and experimental slopes cannot be accounted for by the uncertainty in the effective mass and the deformation potential constant used in the calculation. The effective mass of holes in these structures depends on the strain induced nonparabolocity of the valence band. Samples B and C have different germanium content in the buffer (Table I) and hence different strain in the Ge layers. Therefore, the effective mass in the two samples is not identical. However, we observed that the high-field behavior of both these samples is very similar, suggesting that the effective mass does not significantly affect the rate of decrease of mobility with electric field. However, in an earlier study on hot carrier effects in germanium[8] by Shubnikov de Haas measurements at very low temperatures, significant effects of two-dimensional confinement of phonons in the germanium layers was reported. This was attributed to the acoustic mismatch of the germanium layer with the cladding layers. The modified dispersion relation for the 2D confined phonons manifested itself in the transport properties at the very low lattice (~ 0.3 K) and carrier temperatures (~ 10 K) involved in these experiments. Such an effect was not observed in strained Si channels since according to Snell's law of refraction for acoustic waves, the sound velocities in the active layer need to be smaller than those in the cladding layers to have total internal reflections that confine the phonons. The velocity of acoustic waves is lesser in germanium (5×10^3 m/s) compared to silicon (9×10^3 m/s). This shows that total (or partial) internal reflection appears possible in germanium layers and not in silicon layers. When we took into account the two-dimensional nature of the confined phonons in the Ge channel, we observed that at the energies of interest in our experiments (10–100 K), many modes are excited. When we sum over a very large number of these modes in our calculations, there is no change in the behavior of the high-field mobility from the 3D calculation (dotted line in Fig. 8).

The confinement of the phonons, however, could cause a significant increase in the local temperature of the Ge layer because the confined phonons are not able to reach equilibrium rapidly with the rest of the lattice. This local heating of phonons can be described to first order by a simple linear dependence of the nonequilibrium phonon temperature (T_{ph}) on the bath temperature (T_{bath}) and the carrier temperature (T_c) as

$$T_{ph}=T_{bath}+\alpha(T_c-T_{bath}), \tag{2}$$

with α as the fitting parameter. In such a situation the carrier-phonon scattering is enhanced leading to a faster decrease of mobility at high-electric fields. We repeated the numerical calculations using this nonequilibrium phonon model and obtained the solid line in Fig. 8 for $\alpha=0.3$. This corresponds to a carrier temperature (Tc) of approximately 120 K (inset Fig. 8) and phonon temperature (T_{ph}) of about 30 K at 100 V/cm. Our theoretical calculation along with the experimental results suggests that confined phonons in strained 2D germanium layers sandwiched between SiGe layers may be out of equilibrium with the rest of the lattice at high fields and cause a faster decrease of mobility. A similar conclusion was reached from the experimental data and theoretical calculations for sample #C.

IV. DUTY CYCLE DEPENDENT THERMAL RESPONSE

High-electric fields are known to cause lattice heating, which can cause degradation of mobility apart from the above-mentioned ''hot carrier'' effects. A systematic study of the mobility dependence on the input power will provide a clear understanding of the mechanism of heat transfer in these heterostructures both in transient and in steady-state conditions. In this section we report experimental data on the thermal response of silicon and germanium strained layers by studying the duty cycle dependence of the mobility in these systems at high-electric fields.

In the absence of the electric field the whole system is characterized by the bath temperature (T_{bath}). In the presence of high-electric fields, the carriers reach steady state on a very short time scale (less than picoseconds) and are characterized by the carrier temperature (T_c). These ''hot carriers'' emit phonons that flow through the sample to the bath. In steady state the average temperature of the channel in the presence of the electric-field pulse is characterized by a phonon temperature T_{ph} ($>T_{bath}$). Depending upon the response time of T_{ph} two situations can arise. In the first case where T_{ph} typically has a slow response time of the order of milliseconds as is the case in bulk samples with very large heat capacity, the value of T_{ph} depends on the average energy dissipated in one period of the pulse train and hence,

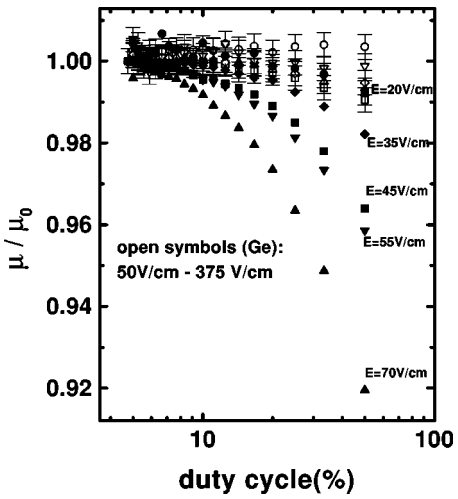

FIG. 9. Normalized mobility vs the duty cycle (%) for different electric fields for the 2DEG sample (#A)—solid symbols and 2DHG sample (#C)—open symbols, at bath temperature of 13 K.

depends on the duty cycle. In the second case where T_{ph} has a very fast time response as is the case in very thin layers, it depends on the instantaneous power dissipated and hence, independent of the duty cycle. A measurement of mobility as a function of the duty cycle thus gives direct information about the thermal response time scales involved.

Pulsed voltages with variable pulse width and frequency were applied to generate high-electric fields. The GMR was used to measure the mobility at each electric field and duty cycle. The electric fields were varied between 10–400 V/cm and duty cycles 1%–50%.

In Fig. 9 we plot the normalized mobility (μ/μ_0) as a function of the applied duty cycle for both the silicon and germanium systems at a bath temperature of 13 K and for different electric fields. The width of the electric-field pulse was kept constant at 200 μs and the period was varied to change the duty cycle.

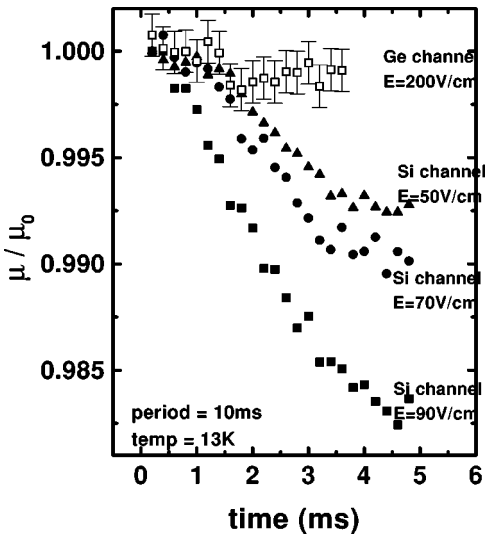

FIG. 10. Normalized mobility as a function of time measured inside a pulse of 5 ms width and 10 ms period (50% duty cycle) for the 2DEG sample (#A)—solid symbols and 2DHG sample (#C)—open symbols, at bath temperature of 13 K.

In the case of silicon samples, we see that the mobility decreased with increasing duty cycle when the bath temperature was fixed at 13 K. The decrease in mobility was more pronounced for higher electric fields. From Fig. 9, for an electric field of 55 V/cm, there is a decrease in mobility by a factor of 0.96 when the duty cycle is varied from 2% to 50%. We see from Fig. 4 that a similar decrease in mobility of 0.96 at a field of 55 V/cm corresponds to an increase in temperature from 13 to 25 K. From this we conclude that the 50% duty cycle pulse causes a local increase of phonon temperature (T_{ph}) to 25 K. A similar analysis at a higher electric field of 70 V/cm, yields a T_{ph} of 40 K at 50% duty cycle and a bath temperature of 13 K. This dependence on the duty cycle shows that the response times in silicon systems are very slow. However, in the case of 2D holes in Ge/SiGe structures (open symbols in Fig. 9), we see that the mobility is relatively independent of the duty cycle even at the highest applied electric fields (380 V/cm). This independence of the mobility on the duty cycle indicates that the time constants are very small in the Ge samples, as discussed above. The time constants in these systems can be estimated by measuring the transient response of mobility inside a pulse of 5 ms width, as shown in Fig. 10. It is observed that the mobility decreases and saturates after few ms in the case of silicon. However, in the case of a germanium sample, no such change is observed within the experimental error, confirming that the time constant is much smaller than a millisecond. This fast time response in germanium can be attributed to the very small heat capacity of the thin germanium layer in which the phonons emitted by the hot carriers are confined. This study confirms the role of confined phonons on the mobility degradation as a function of electric field in the germanium channel, as proposed in the previous section.

There have been few reports in the past to measure the temperature or the distribution of hot carriers experimentally. Shah and Pinczuk *et al.*[33] used the photoluminescence (PL) technique to determine the electron temperature at high-electric fields by fitting the high-energy slope of the PL spectrum to a Fermi–Dirac distribution. In the case of Si–Ge systems, the luminescence is inherently very weak due to the indirect gap in these materials. Also in our case, the PL spectrum is dominated by luminescence from the dislocations in the graded SiGe layer, which makes it even more difficult to study the luminescence from the well. Xie *et al.*[17] and Song *et al.*[8] have done Shubnikov de Haas measurements as a function of temperature (<6 K) to measure the carrier temperature. These measurements have a limitation that they cannot be performed beyond temperatures of about 10 K. Hirakawa *et al.*[35] have studied the broadband far-infrared radiation from hot two-dimensional electrons to determine the black-body temperature. All these techniques have been used to determine the carrier temperature at high-electric fields but they do not provide any information about nonequilibrium phonons in confined systems. Moreover, probes such as Raman spectroscopy, which are sensitive to the phonons, do not have the required sensitivity to measure the small increase of the acoustic phonon temperature (30–50 K) encountered in our experiments.

Detailed modeling to quantitatively estimate these heat capacities and time constants and to experimentally deter-

mine the phonon temperature in these systems is beyond the scope of this paper.

V. CONCLUSION

In conclusion, we have measured the Ohmic mobilities of two systems, 2DEG and 2DHG in strained silicon and strained germanium samples using Hall technique and Van der Pauw geometry. We determine the mobility limiting mechanisms at low temperatures by calculating the mobility contribution from various mechanisms using semiclassical Boltzmann transport theory. We conclude that in the 2DEG samples, in both the high- and low-mobility systems, the low-temperature mobility is limited by remote ionized impurity scattering. In the case of 2DHG samples, on the other hand, the low-temperature mobility is limited by interface roughness scattering. We also conclude that unlike 2DHG in the SiGe channel, wherein, the mobility is limited by alloy scattering, 2DHG in the Ge channel promise extremely large 300 K mobilities (in the absence of parallel conduction) which are larger than the electron mobilities in Si channels.

Geometric magnetoresistance technique was used to measure the mobility as a function of the applied electric field. We observe that the mobility in the germanium system starts decreasing faster at high-electric fields compared to the silicon system. We have also studied the microscopic physics governing hot carrier effects in these systems and have fitted our data using the existing theory of nonlinear transport that takes into account the large drift velocities. While this method was successful in explaining the high-field behavior in silicon channels, it could not account for the experimentally observed higher slope in the case of germanium samples. We proposed a model that emphasizes the role of confined phonons due to acoustic mismatch in the case of SiGe/Ge/SiGe structures. These calculations suggest that phonon confinement effects lead to an increased phonon temperature inside the channel that causes the enhanced mobility degradation.

The lattice heating effects were studied in these systems by measuring the mobility as a function of the duty cycle of the applied electric field. We observe that in the silicon system the mobility decreases with duty cycle, the decrease being more pronounced at higher fields. However, in the germanium system the mobility is independent of the duty cycle, suggesting a smaller time constant in comparison to silicon. We attribute the smaller time constant to the confined phonons in the germanium channel. This confirms the role of confined phonons in hot carrier transport in SiGe/Ge/SiGe modulation doped heterostructures.

ACKNOWLEDGMENTS

The authors thank The Department of Science and Technology and The Council for Scientific and Industrial Research, Government of India for financial support and for the Senior Research Fellowship, respectively.

APPENDIX A: BOLTZMANN TREATMENT FOR LOW- AND HIGH-FIELD TRANSPORT

1. Low-field transport

The electronic state in the channel is characterized by a subband index n and a 2D wave vector $\mathbf{k}=(k_x,k_y)$ along the heterointerface. The ground-state wave function and energy are, respectively, given by

$$\Psi_k(\mathbf{r},z)=f(z)\exp(i\mathbf{k}\cdot\mathbf{r}), \tag{A1}$$

$$E(\mathbf{k})=E_0+\hbar^2k^2/2m_t^*, \tag{A2}$$

where $f(z)$ denotes the envelope wave function, m_t^* the electron effective mass, and $\hbar$ the reduced Planck constant.

In the scattering process of 2D carriers, the momentum conservation in the z direction in the three-dimensional (3D) case is replaced by the integral

$$M_{\mathrm{II}}^2=\int M_{\mathrm{III}}^2|I(q_z)|^2dq_z. \tag{A3}$$

Here, $\mathrm{M_{II}}$ and $\mathrm{M_{III}}$ are the bare scattering matrix element in two dimensions and three dimensions, respectively, q_z is the wave vector normal to the heterointerface, and $I(q_z)$ is defined by

$$I(q_z)\equiv\int f(z)^2\exp(iq_zz)dz. \tag{A4}$$

In the following, we assume that the electrons populate only the lower subband, neglecting the contribution of intersubband scattering. We adopt for $f(z)$ the Fang–Howard variational wave function,

$$f(z)=\sqrt{\frac{b^3z^2}{2}}\exp\left(\frac{-bz}{2}\right), \tag{A5}$$

where the variational parameter b is given by

$$b=\left(\frac{12m_l^*e^2}{\chi_0\epsilon_0\hbar^2}\right)^{1/3}\left(N_{depl}+\frac{11}{32}N\right)^{1/3}, \tag{A6}$$

where m_l^* is the longitudinal effective mass, e is the electronic charge, ϵ_0 is the dielectric permittivity, χ_0 is the static dielectric constant, N_{depl} is the areal density of depletion charges, and N is the density of the 2D electron gas. Substitution of Eq. (A5) in Eq. (A4) yields

$$|I(q_z)|^2=\frac{b^6}{(b^2+q_z^2)^3}. \tag{A7}$$

Since the scattering matrix element M_{III} in three-dimensions are well established, we can calculate M_{II} and the differential scattering cross section $\nu(\theta)$ for various scattering mechanisms. We consider here the ionized-impurity scattering, the acoustic-phonon scattering and interface-roughness scattering.

In these elastic scattering processes the screening effect of the carriers is taken into account by using the screening factor

$$S(q)=1+\frac{e^2F(q)\Pi(q)}{2\chi_0\epsilon_0q}, \tag{A8}$$

where $F(q)$ is the form factor defined by

$$F(q)=\int_0^\infty dz\int_0^\infty dz'[f(z)]^2[f(z')]^2\exp[-q|z-z'|]. \tag{A9}$$

Here,

$$\mathbf{q}=\mathbf{k}_2-\mathbf{k}_1 \tag{A10}$$

is the 2D scattering wave vector from the initial state $\mathbf{k}_1$ to the final state $\mathbf{k}_2$. Using the variational wave function given by Eq. (A5), we obtain for the form factor,

$$F(q)=\frac{b(8b^2+9bq+3q^2)}{8(b+q)^3}. \tag{A11}$$

$\Pi(q)$ is the static polarizability function that depends on both temperature T and q given by

$$\Pi(q,T,\xi)=\int_0^\infty d\xi' \frac{\Pi(q,0,\xi')}{4k_BT\cosh^2[(\xi-\xi')/(2k_BT)]}. \tag{A12}$$

In the above equation, ξ is the Fermi energy and k_B is the Boltzmann constant. $\Pi(q,0,\xi)$ is the polarizability function at $T=0$ given by

$$\Pi(q,0,\xi)=\frac{m_t^*}{\pi\hbar^2}\left\{1-u(q-2k_F)\left[1-\left(\frac{2k_F}{q}\right)^2\right]^{1/2}\right\}, \tag{A13}$$

where $u(x)$ is the usual unit step function and k_F is the Fermi wave vector.

When all the acoustic modes are fully excited the differential scattering cross section due to deformation potential scattering $\nu_{DP}(\theta)$ is

$$\nu_{DP}(\theta)=\frac{3bD^2m_t^*k_BT[1-\cos(\theta)]}{32\pi\hbar^2c_LS^2(q)}, \tag{A14}$$

where D is the deformation potential constant, c_L is the longitudinal elastic constant, and $S(q)$ is the screening factor of the carriers.

The differential scattering cross section due to ionized impurities with the charge Ze is given by

$$\nu_I(\theta)=\frac{m_t^*Z^2e^4}{8\pi\hbar^3\chi_0^2\epsilon_0^2}\int dz_i\left[\frac{F(q,z_i)}{qS(q)}\right]^2 n_i(z_i)[1-\cos(\theta)]. \tag{A15}$$

Here, $n_i(z_i)$ is the impurity distribution and $F(q,z_i)$ is given by

$$F(q,z_i)=\int dz|f(z)|^2\exp(-q|z_i-z|). \tag{A16}$$

The scattering cross section for interface roughness scattering is given by the expression

$$\nu_{IRS}(\theta)=\frac{m_t^*}{2\pi\hbar^3}[1-\cos(\theta)](\Delta\Lambda eF_{eff})^2\exp\left(-\frac{1}{4}q^2\Lambda^2\right). \tag{A17}$$

Here, we have defined the effective field F_{eff} by

$$F_{eff}\equiv\int dz|f(z)|^2\frac{\partial v(z)}{\partial z}=\frac{e}{\epsilon_0\chi_0}\left(\frac{1}{2}N+N_{depl}\right), \tag{A18}$$

where $v(z)$ is the electrostatic potential, Δ is the mean-square deviation of the roughness height, and Λ is the lateral spacial decay rate of the roughness.

The inverse of the momentum relaxation time is given by

$$\frac{1}{\tau(E)}=\int_0^{2\pi}\nu(\theta)d\theta \tag{A19}$$

with

$$\nu(\theta)=\nu_I(\theta)+\nu_{DP}(\theta)+\nu_{IRS}(\theta). \tag{A20}$$

The mobility is then given by

$$\mu=\frac{e}{m^*}\langle\tau\rangle \tag{A21}$$

with

$$\langle\tau\rangle=\frac{\int_0^\infty\tau(E)E[\partial f_0(E)/\partial E]dE}{\int_0^\infty E[\partial f_0(E)/\partial E]dE}. \tag{A22}$$

2. High-field transport

To understand the electron heating process, we have performed calculations following the approach of Price. The differential scattering cross section of 2D electrons with translational wave vector $\boldsymbol{k}$ is expressed as

$$\nu_+(\theta)=\int_{-\infty}^{+\infty}dq_zP|I(q_z)|^2N_q[1-f(E+\hbar\omega_q)] \tag{A23}$$

for phonon absorption,

$$\nu_-(\theta)=\int_{-\infty}^{+\infty}dq_zP|I(q_z)|^2(N_q+1)[1-f(E-\hbar\omega_q)]U \tag{A24}$$

for phonon emission, where $U=u(E-\hbar\omega_q)$ is the usual step function, $P\equiv P(q_{xy},q_z)$ is the scattering probability factor, θ is the scattering angle, and N_q is the phonon occupation number, which is given by

$$N_q=[\exp(\hbar\omega_q/k_BT)-1]^{-1}, \tag{A25}$$

where k_B is the Boltzmann constant. Phonon energy $\hbar\omega_q$ is given by $\hbar u_Lq$ for the longitudinal acoustic (LA) phonon mode. Here u_L is the longitudinal sound velocity and $q=\sqrt{(q_{xy}^2+q_z^2)}$.

The scattering probability factor $P(q_{xy},q_z)$ can be calculated for the acoustic-phonon scattering via deformation potential coupling as

$$P_{DP}(q_{xy},q_z)=\frac{m_t^*D^2(\hbar u_Lq)}{8\pi^2\hbar^3c_L[S(q_{xy},T_e)]^2}, \tag{A26}$$

where D is the deformation potential constant and c_L the longitudinal elastic constant. Since in acoustic-phonon scattering the sound velocity can be assumed to be small compared to the electron velocity, $q_{xy}=2k|\sin(\theta/2)|$. The net energy-loss rate of an electron with energy E is expressed as

$$-\frac{dE}{dt}=-\int_0^{2\pi}\hbar\omega_q[\nu_+(\theta)-\nu_-(\theta)]d\theta \qquad \text{(A27)}$$

and the average energy-loss rate is then given by

$$-\left\langle\frac{dE}{dt}\right\rangle=-\int_0^{\infty}\frac{dE}{dt}f(E)dE\Big/\int_0^{\infty}f(E)dE. \qquad \text{(A28)}$$

APPENDIX B: THE GREEN-FUNCTION APPROACH TO HIGH-FIELD TRANSPORT

Using the procedure given by Lei and Ting, we can derive a force and an energy balance equation for steady state as

$$Ne\mathbf{E}+\mathbf{F}(\mathbf{v})=0, \qquad \text{(B1)}$$

$$\mathbf{v}\cdot\mathbf{F}(\mathbf{v})+W(\mathbf{v})=0, \qquad \text{(B2)}$$

where $\mathbf{v}$ is the expectation value of the center-of-mass velocity, or the average drift velocity of the carriers. The current density is given by

$$\mathbf{J}=Ne\mathbf{v}. \qquad \text{(B3)}$$

In Eqs. (B1) and (B2) $\mathbf{F}(\mathbf{v})$ is the frictional force experienced by the center-of-mass when it moves at a constant speed. It is composed of two parts, due to impurities and due to phonons, respectively.

$$\mathbf{F}(\mathbf{v})=\mathbf{F}_i(\mathbf{v})+\mathbf{F}_p(\mathbf{v}). \qquad \text{(B4)}$$

Their expressions are as follows:

$$\mathbf{F}_i(\mathbf{v})=\sum_{q_{xy}}\int dz\, n_i(z)\times\left|\left(\frac{Ze^2}{2\epsilon_0\chi_0 q_{xy}}\right)F(q_{xy},z)\right|^2\mathbf{q}_{xy}\hat{\Pi}_2(\mathbf{q}_{xy},\mathbf{q}_{xy}\cdot\mathbf{v}), \qquad \text{(B5)}$$

$$\mathbf{F}_p(\mathbf{v})=2\sum_{q_{xy},q_z}|M_{\mathrm{II}}(\mathbf{q}_{xy},q_z)|^2\mathbf{q}_{xy}\hat{\Pi}_2(\mathbf{q}_{xy},\omega_q+\mathbf{q}_{xy}\cdot\mathbf{v})\Delta n. \qquad \text{(B6)}$$

$W(\mathbf{v})$ is the energy transfer rate from electron system to phonon system:

$$W(\mathbf{v})=2\sum_{q_{xy},q_z}|M_{\mathrm{II}}(\mathbf{q}_{xy},q_z)|^2\omega_q\hat{\Pi}_2(\mathbf{q}_{xy},\omega_q+\mathbf{q}_{xy}\cdot\mathbf{v})\Delta n, \qquad \text{(B7)}$$

$$\Delta n=\left[n\left(\frac{\hbar\omega_q}{k_BT}\right)-n\left(\frac{\hbar(\omega_q+\mathbf{q}_{xy}\cdot\mathbf{v})}{k_BT_e}\right)\right], \qquad \text{(B8)}$$

$$M_{\mathrm{II}}(\mathbf{q}_{xy},q_z)=M_{\mathrm{III}}(\mathbf{q}_{xy},q_z)I^*(iq_z). \qquad \text{(B9)}$$

In the above equations, $n_i(z)$ is the impurity volume density at z and $n(x)=1/(e^x-1)$ is the Bose function. T and T_e are the lattice and electron temperature, respectively, and $\hat{\Pi}_2(q_{xy},\Omega)$ is the imaginary part of the Fourier transform of the intrasubband electron-density correlation function in two-dimensional representation. In the case of both Si and Ge, only acoustic phonons contribute to the scattering in the energy range considered. Optical-phonon scattering is not dominant. Only the longitudinal modes give rise to acoustic deformation potential with matrix element

$$|M_{\mathrm{III}}(q)|^2=\frac{D^2(\hbar u_l q)}{2c_l}. \qquad \text{(B10)}$$

*Electronic address: maddy@physics.iisc.ernet.in, venki@physics.iisc.ernet.in

[1] K. Ismail, F.K. LeGoues, K.L. Saenger, M. Arafa, J.O. Chu, P.M. Mooney, and B.S. Meyerson, Phys. Rev. Lett. **73**, 3447 (1994).
[2] F. Schäffler, Semicond. Sci. Technol. **12**, 1515 (1997).
[3] E. Kasper, Surf. Sci. **174**, 630 (1986).
[4] C.M. Engelhardt, D. Többen, M. Aschauer, F. Schäffler, G. Abstreiter, and E. Gornik, Solid-State Electron. **37**, 949 (1994).
[5] Y.H. Xie, D. Monroe, E.A. Fitzgerald, P.J. Silverman, F.A. Thiel, and G.P. Watson, Appl. Phys. Lett. **63**, 2263 (1993).
[6] E. Murakami, K. Nakagawa, A. Nishida, and M. Miyao, IEEE Trans. Electron Devices **41**, 857 (1994).
[7] S. Madhavi, V. Venkataraman, C. W. Liu, and J. C. Sturm, *Proceedings of the Device Research Conference*, Santa Barbara, June 1996, and references therein.
[8] S.H. Song, W. Pan, D.C. Tsui, Y.H. Xie, and D. Monroe, Appl. Phys. Lett. **70**, 3422 (1997).
[9] Th. Vogelsang and K. R. Hofmann, *Proceedings of the Device Research Conference*, Santa Barbara, June 1992.
[10] W.T. Masselink, W. Kopp, T. Henderson, and H. Morkoç, IEEE Electron Device Lett. **6**, 539 (1985).
[11] J.A. Cooper and D.F. Nelson, IEEE Electron Device Lett. **2**, 171 (1981).
[12] K. Ismail, S.F. Nelson, J.O. Chu, and B.S. Meyerson, Appl. Phys. Lett. **63**, 660 (1993).
[13] X.L. Lei and C.S. Ting, Phys. Rev. B **32**, 1112 (1985).
[14] X.L. Lei and C.S. Ting, J. Appl. Phys. **58**, 2270 (1985).
[15] K. Hirakawa and H. Sakaki, Phys. Rev. B **33**, 8291 (1986).
[16] V. Venkataraman, C.W. Liu, and J.C. Sturm, J. Vac. Sci. Technol. B **11**, 1176 (1993).
[17] Y.H. Xie, R. People, J.C. Bean, and K.W. Wecht, Appl. Phys. Lett. **49**, 283 (1986).
[18] P. J. Price, Ann. Phys. **133**, 217 (1981).
[19] F. Schäffler, D. Többen, H-J. Herzog, G. Abstreiter, and B. Holländer, Semicond. Sci. Technol. **7**, 260 (1992).
[20] S. Takagi, J.L. Hoyt, J.J. Welser, and J.F. Gibbons, J. Appl. Phys. **80**, 1567 (1996).
[21] C. Jacoboni and L. Reggiani, Rev. Mod. Phys. **55**, 645 (1983).
[22] B. Laikhtman, Appl. Phys. Lett. **59**, 3021 (1991).
[23] T. Ando, J. Phys. Soc. Jpn. **51**, 3900 (1982).
[24] T. Ando, A.B. Fowler, and F. Stern, Rev. Mod. Phys. **54**, 437 (1982).

[25] H. Sakaki, K. Hirakawa, J. Yoshino, S.P. Svensson, Y. Sekiguchi, T. Hotta, S. Nishi, and N. Miura, Surf. Sci. **142**, 306 (1984).
[26] K. Seeger, *Semiconductor Physics* (Springer, Berlin, 1982).
[27] F. Stern and S.E. Laux, Appl. Phys. Lett. **61**, 1110 (1993).
[28] B. Laikhtman and R.A. Kiehl, Phys. Rev. B **47**, 10 515 (1993).
[29] F.F. Fang and A.B. Fowler, Phys. Rev. B **169**, 619 (1968).
[30] F.F. Fang and A.B. Fowler, J. Appl. Phys. **41**, 1825 (1970).
[31] K. Hess and C.T. Sah, Phys. Rev. B **10**, 3375 (1974).
[32] K. Nakamura, Surf. Sci. **58**, 48 (1976).
[33] J. Shah and A. Pinczuk, Appl. Phys. Lett. **44**, 322 (1984).
[34] K. Hirakawa and H. Sakaki, Appl. Phys. Lett. **49**, 889 (1986).
[35] K. Hirakawa, M. Grayson, D.C. Tsui, and Ç. Kurdak, Phys. Rev. B **47**, 16 651 (1993).